Polish Journal of Medical Physics and Engineering
The Journal of Polish Society of Medical Physics
ISSN 1898-0309, doi: 10.2478/pjmpe-2023-0012

June 2023
Vol 29, Issue 2

Technical Note

Comparison of noise-power spectrum and modulation-transfer function for CT images reconstructed with iterative and deep learning image reconstructions: An initial experience study

Adiwasono M. B. SETIAWAN[1,BCDF], Choirul ANAM[1,ACEF,*], Eko HIDAYANTO[1,BCEF], Heri SUTANTO[1,BCEF], Ariij NAUFAL[1,BCEF], Geoff DOUGHERTY[2,CEF]

[1]*Department of Physics, Faculty of Sciences and Mathematics, Diponegoro University, Jl. Prof. Soedarto SH, Tembalang, Semarang 50275, Central Java, Indonesia*

[2]*Department of Applied Physics and Medical Imaging, California State University Channel Islands, Camarillo, CA 93012, USA*

[*]*Corresponding author: Dr. Choirul Anam; anam@fisika.fsm.undip.ac.id*

(received 20 March 2023; accepted 4 May 2023)

Abstract

Introduction: Deep learning image reconstruction (DLIR) is a very recent image reconstruction method that is already available for commercial use. We evaluated the quality of DLIR images and compared it to the quality of images from the latest adaptive statistical iterative reconstruction (ASIR-V) algorithm in terms of noise-power spectrum (NPS) and modulation-transfer function (MTF).

Methods: We scanned a Revolution QA phantom (GE Healthcare, USA) and a 20 cm water phantom (GE Healthcare, USA) with our 512 multi-slice computed tomography (CT) scanner. Images of the tungsten wire within the Revolution QA phantom were reconstructed with a 50 mm field of view (FOV). The images were reconstructed with various ASIR-V strengths (i.e. 0, 10, 20, 30, 40, 50, 60, 70, 80, 90, 100%) and DLIRs (i.e. low, medium, and high) to assess the MTF. The images from the 20 cm water phantom were reconstructed with the same configuration to assess the NPS.

Results: The MTF was similar for both reconstruction algorithms of DLIR and ASiR-V. The peak frequency (f_p) of the DLIR low was comparable to that from ASIR-V at 50, 60, 70%; the DLIR medium was comparable to ASIR-V at 80%; and the DLIR high was comparable to ASIR-V at 100%. The average frequency (f_A) of the DLIR low was comparable to that from ASIR-V at 40%; the DLIR medium was comparable to ASIR-V at 50%; and the DLIR high was comparable to ASIR-V at 70%. Both the DLIR and ASIR-V were able to reduce noise, but they had a different texture.

Conclusions: The noise in the DLIR images was more homogenous at high and low frequencies, while in the ASIR-V images, the noise was more concentrated at high frequencies. The MTF was similar for both reconstruction algorithms. The DLIR method showed a better noise reduction than the ASIR-V reconstruction.

Keywords: ASIR-V; DLIR; noise power spectrum; modulation transfer function.

Introduction

Computed tomography (CT) scan is an excellent medical imaging tool for visualizing and quantifying internal structures within the human body.[1] Because CT scan uses ionization radiation, radiation dose must be kept to a minimum, while maintaining image quality.[2] Many studies have reported that modifications in reconstruction algorithms have a major impact on image quality,[3-6] along with the development of CT scan hardware technology. Image reconstruction technology has progressed in order to deliver high-quality images at low patient doses and faster reconstruction times.[7,8] Advances in CT image reconstruction aim to achieve the perfect triad of high-quality images at low patient doses with fast reconstruction speeds.[8]

Initially, CT scan imaging used the algebraic reconstruction technique (ART).[9] This reconstruction makes no assumptions about the absolute value of the patient's attenuation nor the frequency content in the patient's body. Hence, it cannot distinguish areas that should not undergo noise reduction, such as areas with high-frequency content where a reduction in spatial resolution would be undesirable.[9] Along with the development of computer hardware and software, the ART algorithm was replaced by filtered back-projection (FBP), which is now widely available. One of the major drawbacks of the FBP method is the high level of noise and streak artifacts that lead to low signal-to-

© 2023 Authors This is an open access article licensed under the Creative Commons Attribution-NonCommercial-NoDerivs License (http://creativecommons.org/licenses/by-nc-nd/4.0/).

Authors' contribution: A – Research concept and design, B – Collection and/or assembly of data, C – Data analysis and interpretation, D – Writing the article, E – Critical revision of the article, F – Final approval of the article.

noise ratio (SNR) and contrast-to-noise ratio (CNR).[8] Noise increases in proportion to the inverse square root of the dose or the slice thickness in the CT acquisition.[9] FBP tends to need a higher radiation dose to produce low-noise CT images.[10] For example, FBP requires four times the radiation dose to reduce the noise by 50%.

The shortcomings of FBP prompted various vendors to develop an image reconstruction method called iterative reconstruction (IR) in 2008.[11] IR has the ability to identify anatomical regions of high spatial frequency content and minimize spatial resolution degradation. Its ability to selectively reconstruct different regions within images made IR as powerful noise-reducing method.[9] However, the noise reduction process in IR altered the image texture, which radiologists often referred to as "smooth", "blotchy" or "plastic looking" .[12,13]

To overcome these shortcomings, image reconstruction based on artificial intelligence (AI), called the deep learning image reconstruction (DLIR) method, was developed.[8,14] DLIR can reduce noise to a similar level to IR but also can optimize the image texture that had become a problem in the IR algorithm. Theoretically, DLIR can also be used to solve various image reconstruction problems, including cone-beam artifacts, motion artifacts, truncation and so on. Currently, commercially available DLIRs are now focused on noise reduction.[9]

DLIR is a relatively new algorithm.[15-17] DLIR has just been installed in our institution. Therefore, as an initial experience, it is very interesting to characterize its behavior, especially in producing image texture when compared to IR. By evaluating the image quality, we can understand the characteristics of the DLIR method compared to other reconstruction methods.[18] Knowledge of the advantages and disadvantages of DLIR will be useful for optimizing exposure factors in clinical applications.[19] As an initial study, we compared the adaptive statistical iterative reconstruction method (ASIR-V) and the DLIR algorithm developed by GE using two important image quality parameters, i.e., noise and spatial resolution.[14] The noise was represented by the noise-power spectrum (NPS) for a more comprehensive description of the noise texture.[21-24] The modulation-transfer function (MTF) was used for spatial resolution.[25-27]

Methods

Phantom and image reconstruction

We used two types of phantoms, i.e. the 20 cm water phantom (GE Healthcare, USA) for NPS evaluation and the Revolution QA phantom (GE Healthcare, USA) for MTF evaluation. We used scan parameters that are routinely used for annual CT image quality control. The scan parameters used are shown in **Table 1**.

The image results obtained from the 20 cm water phantom were reconstructed with a thickness of 0.625 mm using two types of image reconstruction, i.e. ASIR-V with various strengths (10, 20, 30, 40, 50, 60, 70, 80, 90, and 100%) and DLIR (low, medium, and high). Meanwhile, the images obtained from the Revolution QA phantom were reconstructed for a 0.05 mm diameter tungsten wire in the phantom with a 50 mm field of view (FOV) for MTF measurements. **Figure 1** shows the images of the water phantom, and **Figure 2** shows the images of the Revolution QA phantom.

NPS and MTF measurements

The standard deviation (SD) is used for determining the noise magnitude. The visual impression of image noise (e.g. fine, or coarse) as a result of noise correlations introduced during the image reconstruction process is referred to as noise texture.[22] The noise texture can be characterized using NPS. NPS across the image FOV can be measured in a homogeneous region of the water phantom. NPS measurements were performed using the ImQuest software (Duke University, Durham, NC, USA),[28] with five regions of interest (ROIs) of 64 pixels. The NPS was measured as the average from 55 slices. The peak frequency (f_p) and the average frequency (f_A) were used to determine noise texture which describes the overall frequency content of the NPS.

$$f_P = \arg max[NPS(f)] \quad \text{Eq. 1}$$

and

$$f_A = \frac{\int f \cdot NPS(f)\, df}{\int NPS(f)\, df} \quad \text{Eq. 2}$$

where f is the radial spatial frequency, and NPS(f) is the radially re-binned/average 1D NPS.

Table 1. Scan parameters.

Parameter	Value
Scanner	GE Apex
Tube current (mAs)	340
Tube voltage (kVp)	120
Detector coverage (mm)	40/80
Scan mode	Axial
Rotation time (s)	1
Convolution kernel	Standard
Image reconstruction	ASIR-V and DLIR

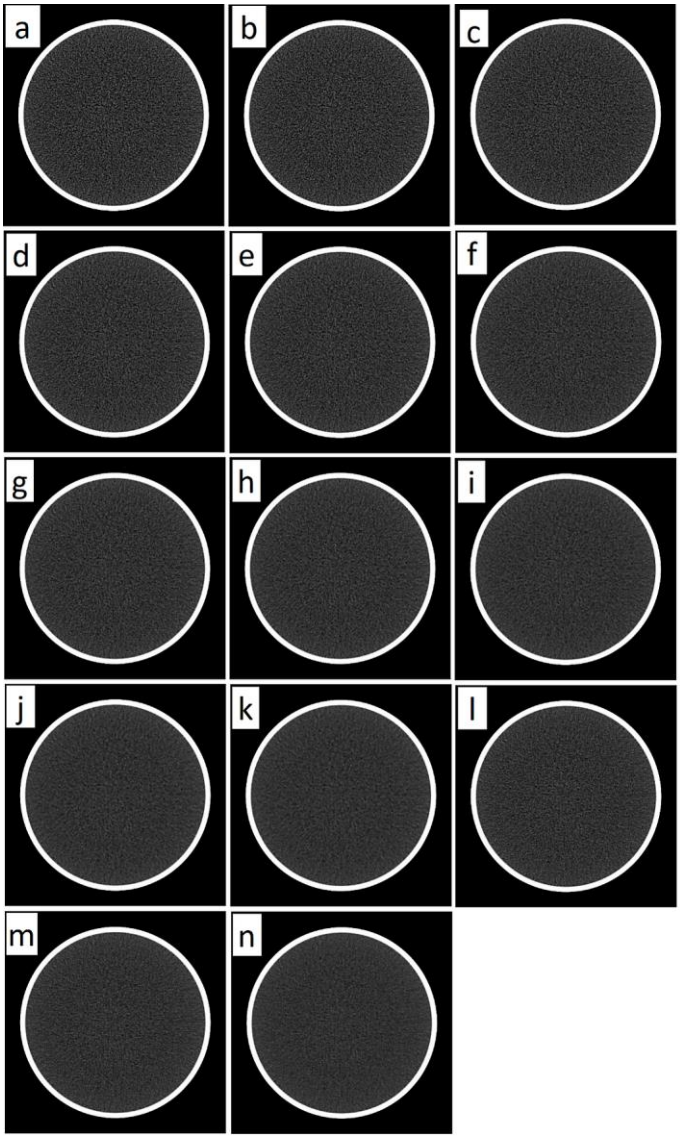


Figure 1. Sample images of the 20 cm water phantom with various ASIR-V values and DLIR; (a) ASIR-V 0%, (b) ASIR-V 10%, (c) ASIR-V 20%, (d) ASIR-V 30%, (e) ASIR-V 40%, (f) ASIR-V 50%, (g) ASIR-V 60%, (h) ASIR-V 70%, (i) ASIR-V 80%, (j) ASIR-V 90%, (k) ASIR-V 100%, (l) DLIR low, (m) DLIR medium, and (n) DLIR high.

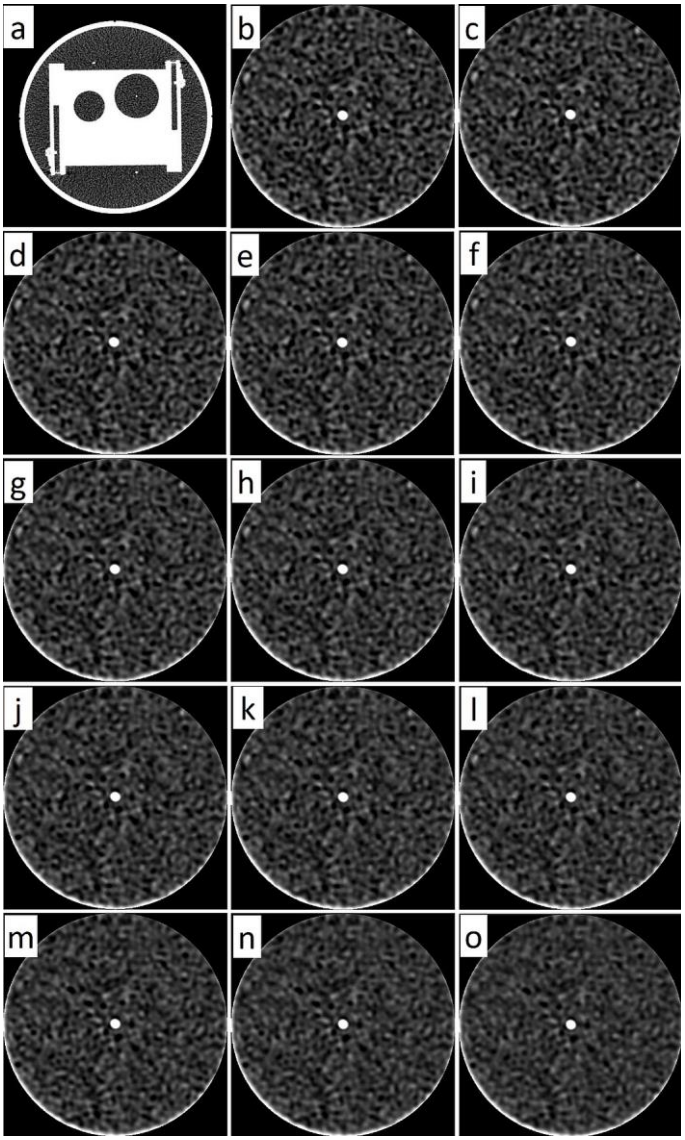


Figure 2. Sample images of the Revolution QA phantom with various ASIR-V values and DLIR at 50 mm FOV; (a) original sample of 250 mm FOV, (b) ASIR-V 0%, (c) ASIR-V 10%, (d) ASIR-V 20%, (e) ASIR-V 30%, (f) ASIR-V 40%, (g) ASIR-V 50%, (h) ASIR-V 60%, (i) ASIR-V 70%, (j) ASIR-V 80%, (k) ASIR-V 90%, (l) ASIR-V 100%, (m) DLIR low, (n) DLIR medium, and (o) DLIR high.

Figure 3 depicts the ROI positions for NPS measurement. To investigate the shift in image noise texture, the NPS measurement results were normalized by dividing all measured data by the maximum frequency value for each image reconstruction variation.

The IndoQCT software[29] was used to perform the MTF measurements automatically. The point MTF method was used[30,31] with a ROI of 64 pixels on the tungsten wire object using reconstructed images of the Revolution QA phantom at a FOV of 50 mm, as shown in **Figure 4**. For the 50 mm FOV and a 512-image matrix, the size of each pixel is 50 mm / 512 = 0.0977 mm ≈ 0.1 mm. The Nyquist frequency is expressed as 1/2d, with d is the pixel size. Hence, for this FOV, the Nyquist frequency will be around 5 cycles/mm. This FOV is appropriate for measuring MTF because the spatial resolution of many CT scanners is within the range of 0.5-2 cycle/mm.[32]

For automated MTF calculation, the image of the point object was at the center of the region of interest (ROI) and it was cropped to 64 × 64 pixels. To get a pixel profile along the y-axis, we summed along the x-direction (*S(x)*).

$$S(x) = \sum_{ymin}^{ymax} ROI\ (x, y) \qquad \text{Eq. 3}$$

To make sure that the profile had a zero tail, a zeroing process was performed. This was done by calculating the mean value of 5 pixels on both the right and left side of the profile ($S(x)$), using **Equation 4**.

$$\overline{S(x_{10})} = \frac{\sum_{i=1}^{5} S(x_i) + \sum_{i=n-5}^{n} S(x_i)}{10} \qquad \text{Eq. 4}$$

Then all points on *S(x)* were reduced by $\overline{S(x_{10})}$.

$$S'(x) = S(x) - \overline{S(x_{10})} \qquad \text{Eq. 5}$$

The next step was to normalize the curve so that the total data was equal to unity, to ensure that the MTF value at zero spatial frequency is 1.0.[20] The normalization process was done by dividing all points on the $S'(x)$ curve with the total value of $S'(x)$.

$$LSF(x) = \frac{S'(x)}{\sum_{i=1}^{n} S'(x_i)} \qquad \text{Eq. 6}$$

The distance between pixels was used to convert the x-axis in the LSF curve from pixel number to distance in mm (or cm). The distance between pixels was found from the DICOM header. Finally, the MTF curve was found from the Fourier transform of the LSF curve.

$$MTF(f) = \left|F\left(LSF(x)\right)\right| = \left|\int_{-\infty}^{+\infty} [LSF(x) e^{-2\pi j x f}]\, dx\right| \qquad \text{Eq. 7}$$

where *f* represents the spatial frequency, and *F* represents the Fourier transform.

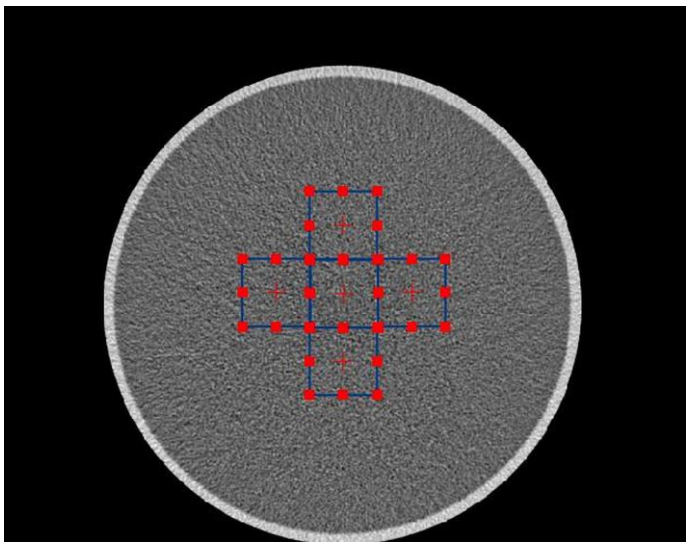


Figure 3. NPS measurement using five regions of interests (ROIs).

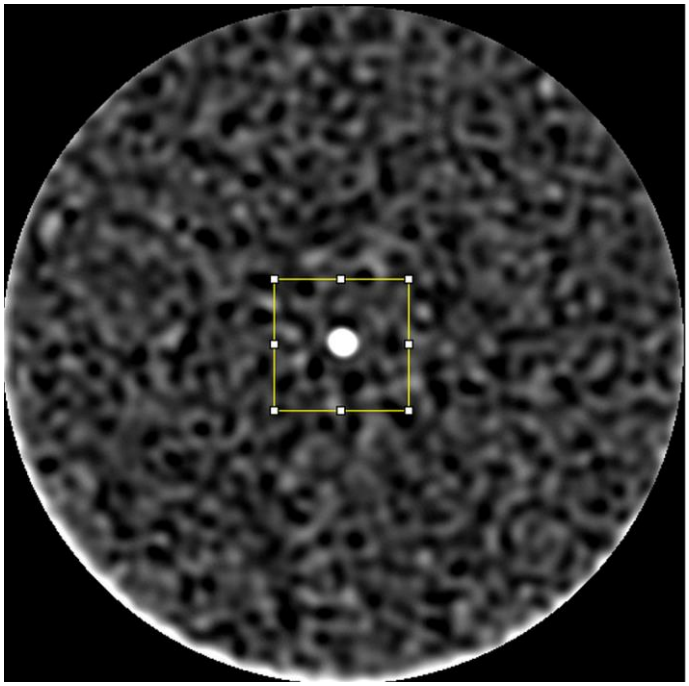


Figure 4. MTF measurement using ROI centered on the tungsten wire of the Revolution QA phantom.

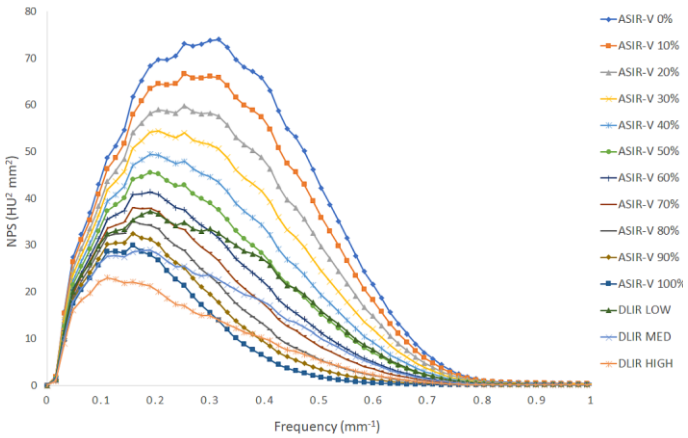


Figure 5. NPS curves for various ASIR-Vs and DLIRs.

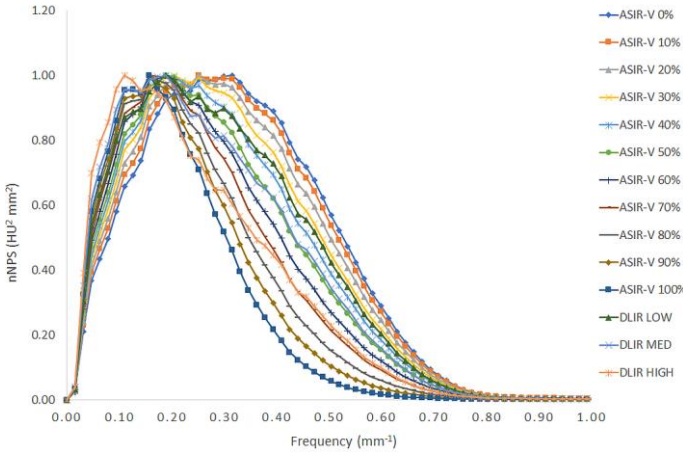


Figure 6. Normalized NPS curves for various ASIR-Vs and DLIRs.

Results

NPS measurement results

Figure 5 shows the NPS curves for various ASIR-Vs and DLIRs. The ASIR-V reconstruction image shows a general reduction in noise with incrementing ASIR-V value (i.e. from 0 to 100%), as does the use of DLIR (low, medium, high). All NPS curves show a shift towards lower frequencies with increasing ASIR-V values or when DLIR goes from low to medium and high. The NPS curves show a different texture shape between ASIR-V and DLIR. **Figure 6** depicts the normalized NPS curves. The normalized NPS curves clearly indicate the f_p of the NPS curves.

The average noise level in Hounsfield units (HU) was reduced by 0.5 HU or 8.8% for each addition of 10% in the ASIR-V value. For the three DLIR images with variations of low, medium, and high, the average noise value was reduced by 0.95 HU or 24.3%, as shown in **Figure 7a**. The noise magnitude of DLIR low is comparable to ASIR-V at 50%, DLIR medium to ASIR-V at 70%, and DLIR high to ASIR-V at 100%, and is 5.4, 4.5 and 3.5 HU, respectively. The percentage noise reduction for the ASIR-V and DLIR images compared to the original image (ASIR-V 0%) is shown in **Figure 7b**. It also shows that noise reduction of DLIR low is comparable to ASIR-V at 50%, DLIR medium to ASIR-V at 70%, and DLIR high to ASIR-V at 100%, and is 34.9, 45.8, and 57.8%, respectively. Due to DLIR's noise reduction properties, it is now possible to exploit the new spatial resolution limit with a detector of a smaller pixel size and a sharper kernel with a larger image matrix without causing a noise penalty.[9]

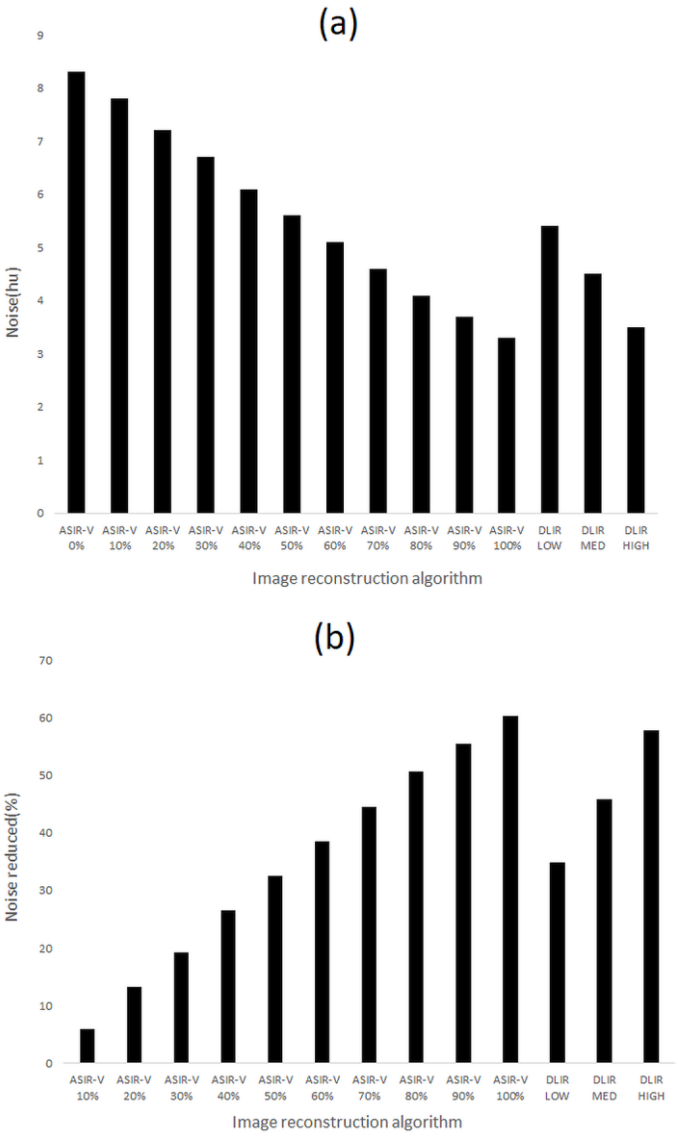


Figure 7. (a) Noise level with ASIR-V and DLIR variation. (b) Percentage of reduced noise compared to the original image (ASIR-V 0%).

Figure 8 shows the f_p and f_A for both the ASIR-V and DLIR reconstructions. The f_p tends to decrease with increasing ASIR-V strength. This shows the effectiveness of ASIR-V in reconstructing images with low noise. The f_p at low DLIR is similar to that for ASIR-V 50, 60, 70%, the medium DLIR is similar to ASIR-V 80%, and the high DLIR is similar to ASIR-V 100%.

The f_A value also shows a decrease with increments of ASIR-V strength and changes in DLIR low, medium, and high variations. The f_A value at DLIR low is similar to the f_A value at ASIR-V 40%, DLIR medium is similar to ASIR-V 50%, and DLIR high value is similar to ASIR-V 70%. As ASIR and DLIR increase, the f_A decreases from ~0.30 to ~0.25 mm^{-1}. For both reconstructions, increased strength produces more noise at lower frequencies.

MTF measurement results

Figure 9 shows the MTF curves for various ASIR-Vs and DLIRs. There is no significant change in the MTF curves for different ASIR-V strengths (0 – 100%). This is also observed in the DLIR images at various strengths (low, medium, and high). MTF curves provide information across all spatial frequencies of interest. MTF curves that coincide with each other indicate similar spatial resolution characteristics at all frequencies. This demonstrates the capability of both ASIR and DLIR reconstructions to maintain spatial resolution while reducing noise at various reconstruction strengths.[33] In this study, we only used one value of radiation dose, which has no effect on spatial resolution. If the radiation dose is high enough, the noise filter within the image reconstruction does not have to perform as hard, so the MTF is almost the same. If the radiation dose is low, a strong noise reduction will blur the image and decrease the MTF.[31] **Figure 10** shows that the average value of MTF 50 obtained was 0.3 mm^{-1} and MTF 10 was 0.65 mm^{-1} for all variations of ASIR-V and DLIR.

Discussion

DLIR is the most recent image reconstruction algorithm commercially available. In order to optimize its clinical applications, it is necessary to evaluate the image quality and compare it to the previous image reconstruction algorithm. The comparison of reconstructed images between DLIR and ASIR-V in this study shows that the noise in the DLIR image is typically lower than that in the ASIR-V image. This can be seen from the NPS of DLIR images, where noise is distributed more evenly across all frequency ranges, whereas the noise in the ASIR-V images is more concentrated at high frequencies. When using noise reduction reconstruction algorithms, reducing low frequencies tends to be difficult, and the proportion of low-frequency components in the NPS curves tends to increase.

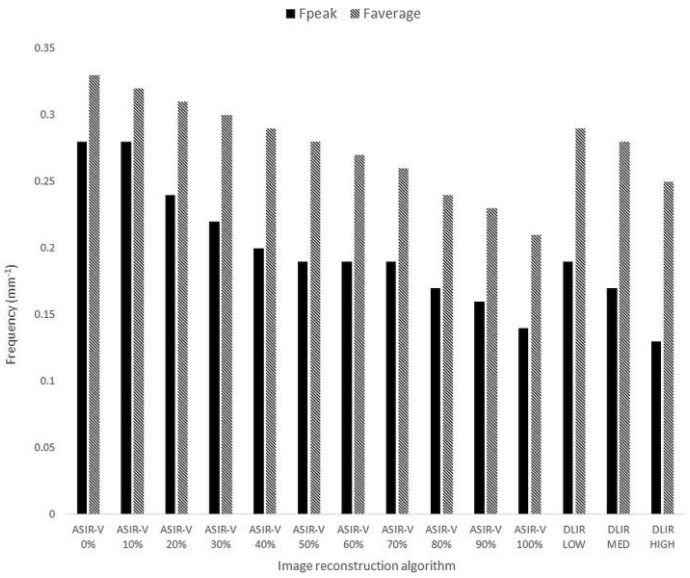


Figure 8. f_p and f_A with ASIR-V and DLIR variations.

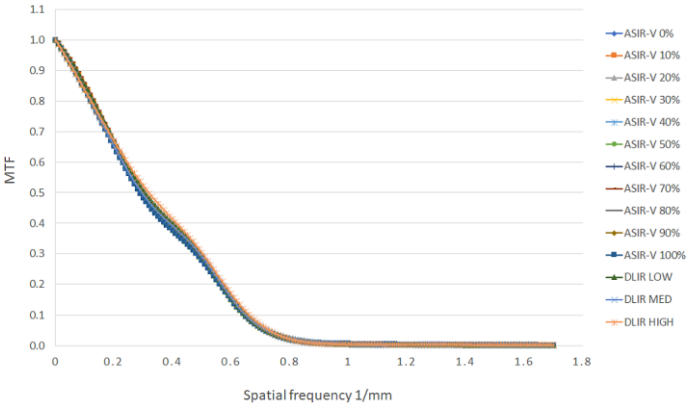


Figure 9. MTF curves for ASIR-V and DLIR variations.

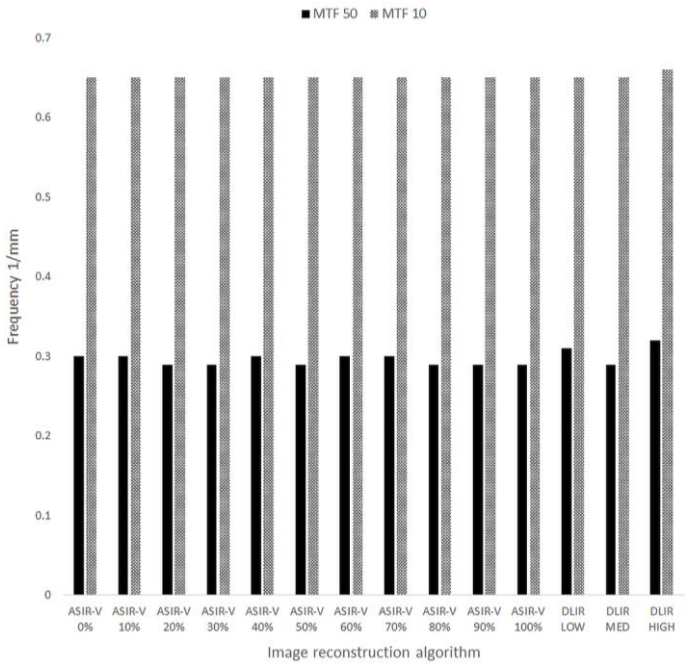


Figure 10. MTF 10 and MTF 50 values for variations of ASIR-V and DLIR.

Increasing low-frequency components results in a coarsening of image texture, i.e., it will look "plastic-like" or "cartoony", which will compromise the detection of small lesions.[31] In the DLIR images, even low-frequency components were suppressed effectively. This makes DLIR superior to ASIR-V in this regard, with the appearance of the DLIR image looking sharper than ASIR-V. This has the potential to be used for dose reduction in the future without compromising image sharpness. The changes in noise texture between DLIR and ASIR-V are in accordance with previous reports.[33,34] Due to DLIR's noise reduction properties, it is now possible to exploit the new spatial resolution limit with a detector of smaller pixel size and using a sharper kernel with a larger image matrix without causing a noise penalty.[9]

ASIR-V can drastically reduce noise at high frequencies (0.4-0.6 mm^{-1}), whereas DLIR produces more noise at this frequency. However, at low frequencies (0.05-0.1 mm^{-1}), DLIR performs better than ASIR-V at noise reduction.[35] Low-frequency noise texture is affected by iterative reconstruction techniques with higher iteration[36] and has shown to be a clinical limitation for some imaging tasks. Iteratively reconstructed objects that are overly smooth will give the impression of unnatural noise and make low contrast detection more difficult.[36,37] It is hoped that these issues will be resolved by reducing the low-frequency noise in DLIR images. The impact of the reduced noise generated in both these reconstructions on low-contrast detectability is very interesting and needs to be investigated further because noise directly affects low-contrast lesions.[34]

The comparison of the spatial resolution between ASIR-V and DLIR images shows that variations in the ASIR-V and DLIR strength do not show any significant change in the values of MTF 10 and MTF 50. As previously reported,[17] MTF 10 and MTF 50 with variations in ASIR of 20, 40, 60, 80 and 100% are comparable. The MTF curves are hardly distinguishable. This indicates that both image reconstructions (ASIR-V and DLIR) can maintain spatial resolution.

In this study, the image quality assessment was only performed using available vendor phantoms, i.e. the Revolution QA phantom and the 20 cm water phantom. These phantoms do not provide a variable multi-pin insert: hence the task-transfer function (TTF) was not performed to assess spatial resolution at various contrasts and noise levels.[13,22] We will investigate this in the future with a dedicated phantom to evaluate the effect of both image reconstructions on TTF. We only used a single dose and a standard kernel, and have not yet investigated variations in radiation dose or the effect of using different kernel filters on image quality, which would change the frequency distribution of the image noise and spatial resolution.[13,38]

Conclusions

We compared the ASIR-V and the DLIR developed by GE using two important image quality parameters, i.e. noise represented by the NPS and spatial resolution represented by MTF. These two parameters were determined using CT images with varying iterative reconstruction strengths and levels of deep learning image reconstruction. The DLIR method shows a better noise reduction because it maintains better noise texture than the ASIR-V reconstruction. DLIR is superior to ASIR-V in terms of noise reduction at low-frequency components, resulting in a sharper DLIR image. Spatial resolution is not affected by the image reconstruction methods for both ASIR-V and DLIR for any strength of iterative reconstruction and level of deep learning image reconstruction.

Funding

This work was funded by the Riset Publikasi Internasional (RPIT), Diponegoro University. No. 569-114/UN7-D2/PP/IV/2023

Conflicts of Interest

The authors declare no conflict of interest.

References

1. Yim D, Lee S, Nam K, Lee D, Kim KD, Kim J S. Deep learning-based image reconstruction for few-view computed tomography. Nuclear Instruments and Methods in Physics Research Section A: Accelerators, Spectrometers, Detectors and Associated Equipment. 2021;1011:166594. https://doi.org/10.1016/j.nima.2021.165594
2. Anam C, Naufal A, Fujibuchi T, Matsubara K, Dougherty G. Automated development of the contrast-detail curve based on statistical low-contrast detectability in CT images. J Appl Clin Med Phys. 2022;23:e13719. https://doi.org/10.1002/acm2.13719
3. Li K, Tang J, Chen GH. Statistical model based iterative reconstruction (MBIR) in clinical CT systems: experimental assessment of noise performance. Med Phys. 2014;41:041906. https://doi.org/10.1118/1.4867863
4. Morsbach F, Desbiolles L, Raupach R, Leschka S, Schmidt B, Alkadhi H. Noise texture deviation: a measure for quantifying artefacts in computed tomography images with iterative reconstruction. Invest Radiol. 2017;52:87-94. https://doi.org/10.1097/RLI.0000000000000312

5. Solomon J, Samei E. Quantum noise properties of CT images with anatomical textured backgrounds across reconstruction algorithms: FBP and SAFIRE. Med Phys. 2014;41:091908. https://doi.org/10.1118/1.4893497
6. Andersen HK, Volgyes D, Martinsen ACT. Image quality with iterative reconstruction techniques in CT of the lungs: a phantom study. Eur J Radiol Open. 2018;5:35-40. https://doi.org/10.1016/j.ejro.2018.02.002
7. Willemink MJ, Noël PB. The evolution of image reconstruction for CT-from filtered back projection to artificial intelligence. Eur J Radiol. 2019;29:2185-2195. https://doi.org/10.1007/s00330-018-5810-7
8. Mcleavy CM, et al. The future of CT: Deep learning reconstruction. Clin Radiol. 2021;76:407-415. https://doi.org/10.1016/j.crad.2021.01.010
9. Szczykutowicz PT, Toia VG, Dhanantwari A, Nett B. A review of deep learning CT reconstruction: Concepts, limitations, and promise in clinical practice. Curr Radiol Rep. 2022;10:101-115. https://doi.org/10.1007/s40134-022-00399-5
10. Kataria B, Nilsson AJ, Smedby Ö, Persson A, Sökjer H, Sandborg M. Image quality and potential dose reduction using advanced modeled iterative reconstruction (ADMIRE) in abdominal CT - A review. Radiat Prot Dosim. 2021;195:177-187. https://doi.org/10.1093/rpd/ncab020
11. Greffier J, Frandon J, Larbi A, Om D, Beregi PJ, Perreira F. CT Iterative reconstruction algorithm: A task-based quality assessment. Eur Radiol. 2020;30:487-500. https://doi.org/10.1007/s00330-019-06359-6
12. Greffier J, Franfond J, Si-Mohamed S, et al. Comparison of two deep learning image reconstruction algorithms in chest CT images: A task-based image quality assessment on phantom data. Diagn Interv Imaging. 2022;103:21-22. https://doi.org/10.1016/j.diii.2021.08.001
13. Greffier J, Hamard A, Pereira F, et al. Image quality and dose reduction opportunity of deep learning image reconstruction algorithm for CT: A phantom study. Eur Radiol. 2020;30:3951-3959. https://doi.org/10.1007/s00330-020-06724-w
14. Benz DC, Benetos G, Rampidis G, et al. Validation of deep-learning image reconstruction for coronary computed tomography angiography: Impact on noise, image quality and diagnostic accuracy. J Cardiovasc Comput Tomogr. 2020;14:444-451. https://doi.org/10.1016/j.jcct.2020.01.002
15. Kim JH, Yoon HJ, Lee E, Kim I, Cha YK, Bak SH. Validation of deep-learning image reconstruction for low-dose chest computed tomography scan: Emphasis on image quality and noise. Korean J Radiol. 2021;22:131-138. https://doi.org/10.3348/kjr.2020.0116
16. Wang H, Li LL, Shang J, Song J, Liu B. Application of deep learning image reconstruction in low-dose chest CT scan. Br J Radiol. 2022;95:20210380. https://doi.org/10.1259/bjr.20210380
17. Zahro MU, Anam C, Budi WS, et al. Investigation of noise level and spatial resolution of CT images filtered with a selective mean filter and its comparison to an adaptive statistical iterative reconstruction. Iran J Med Phys. 2021;18:374-383. https://doi.org/10.22038/ijmp.2020.48813.1786
18. Hsieh J, Liu E, Nett B, Tang J, Thibault BJ, Sahney S. A new era of image reconstruction: True Fidelity™ Technical White Paper on Deep Learning Image Reconstruction. GE Healthcare. 2019. https://www.gehealthcare.com/-/jssmedia/040dd213fa89463287155151fdb01922.pdf
19. Szczykutowicz PT, Nett B, Cherkezyan L, et al. Protocol optimization considerations for implementing deep learning CT reconstruction. Am J Radiol. 2021;216:1668-1677. https://doi.org/10.2214/AJR.20.23397
20. Anam C, Fujibuchi T, Haryanto F, et al. Automated MTF measurement in CT images with a simple wire phantom. Pol J Med Phys Eng. 2019;25:179-187. https://doi.org/10.2478/pjmpe-2019-0024
21. Li G, Liu X, Dodge C T, Jensen CT, Rong XJ. A noise power spectrum study of a new model-based iterative reconstruction system: Veo 3.0. J Appl Clin Med Phys. 2016;17:428-439. https://doi.org/10.1120/jacmp.v17i5.6225
22. Samei E, Bakalyar D, Boedeker KL, et al. Performance evaluation of computed tomography systems. Med Phys. 2019;46:735-756. https://doi.org/10.1002/mp.13763
23. Hasegawa A, Ishihara T, Thomas MA, Pan T. Noise reduction profile: A new method for evaluation of noise reduction techniques in CT. Med Phys. 2022;49:186-200. https://doi.org/10.1002/mp.15382
24. Anam C, Arif I, Haryanto F, et al. An improved method of automated noise measurement system in CT images. J Biomed Phys Eng. 2019;11:163-174. https://doi.org/10.31661%2Fjbpe.v0i0.1198
25. Kayugawa A, Ohkubo M, Wada S. Accurate determination of CT point-spread-function with high precision. J Appl Clin Med Phys. 2013;14:3905. https://doi.org/10.1120/jacmp.v14i4.3905
26. Anam C, Fujibuchi T, Budi WS, Haryanto F, Dougherty G. An algorithm for automated modulation transfer function measurement using an edge of a PMMA phantom: Impact of field of view on spatial resolution of CT images. J Appl Clin Med Phys. 2018;19:244-252. https://doi.org/10.1002/acm2.12476
27. Anam C, Naufal A, Sutanto H, Adi K, Dougherty G. Impact of iterative bilateral filtering on the noise power spectrum of computed tomography images. Algorithms. 2022;15:374. https://doi.org/10.3390/a15100374
28. ImQuest. https://deckard.duhs.duke.edu/~samei/tg233.html

29. Anam C, Naufal A, Fujibuchi T, Matsubara K, Dougherty G. Automated development of the contrast-detail curve based on statistical low-contrast detectability in CT images. J Appl Clin Med Phys. 2022;23:e13719. https://doi.org/10.1002/acm2.13719
30. Verdun FR, Racine D, Ott JG, et al. Image quality in CT: From physical measurements to model observer. Phys Med. 2015;31:823-843. https://doi.org/10.1016/j.ejmp.2015.08.007
31. Higaki T, Nakamura Y, Zhou J, et al. Deep learning reconstruction at CT: Phantom study of the image characteristic. Acad Radiol. 2020;27: 82-87. https://doi.org/10.1016/j.acra.2019.09.008
32. Anam C, Naufal A, Sutanto H, Dougherty G. Computational phantoms for investigating impact of noise magnitude on modulation transfer function. Indonesian J Elec Eng Comp Sci. 2022;27:1428-1437. https://doi.org/10.11591/ijeecs.v27.i3.pp1428-1437
33. Racine D, Becce F, Viry A, et al. Task-based characterization of deep learning image reconstruction and comparison with filtered back-projection and partial mode-based iterative reconstruction in abdominal CT: A phantom study. Phys Med. 2020;76:28-37. https://doi.org/10.1016/j.ejmp.2020.06.004
34. Racine D, Brat HG, Dufour B, et al. Image texture, low contrast liver lesion detectability and impact on dose: Deep learning algorithm compare to partial mode-based iterative reconstruction. Eur J Radiol. 2021;141:190808. https://doi.org/10.1016/j.ejrad.2021.109808
35. Greffier J, Frandon J, Durand Q, et al. Contribution of an artificial intelligence deep-learning reconstruction algorithm for dose optimization in lumbar spine examination: A phantom study. Diagn Interv Imaging. 2022;1-8. https://doi.org/10.1016/j.diii.2022.08.004
36. Solomon J, Daniele M, Lyu P, Samei E. Noise and spatial resolution properties of a commercially available deep learning-based CT reconstruction algorithm. Med Phys. 2020;47:3961-3970. https://doi.org/10.1002/mp.14319
37. Papadakis EA, Damilakis J. Technical note: Quality assessment of virtual monochromatic spectral images on a dual energy CT scanner. Phys Med. 2021;82:114-121. https://doi.org/10.1016/j.ejmp.2021.01.079
38. Sugisawa K, et al Technical note: Spatial resolution compensation by adjusting the reconstruction kernels for iterative reconstruction images of computed tomography. Phys Med. 2020;74:47-55. https://doi.org/10.1016/j.ejmp.2020.05.002